Chem

CellPress

Article

Generalized Kasha's Model: *T*-Dependent Spectroscopy Reveals Short-Range Structures of 2D Excitonic Systems

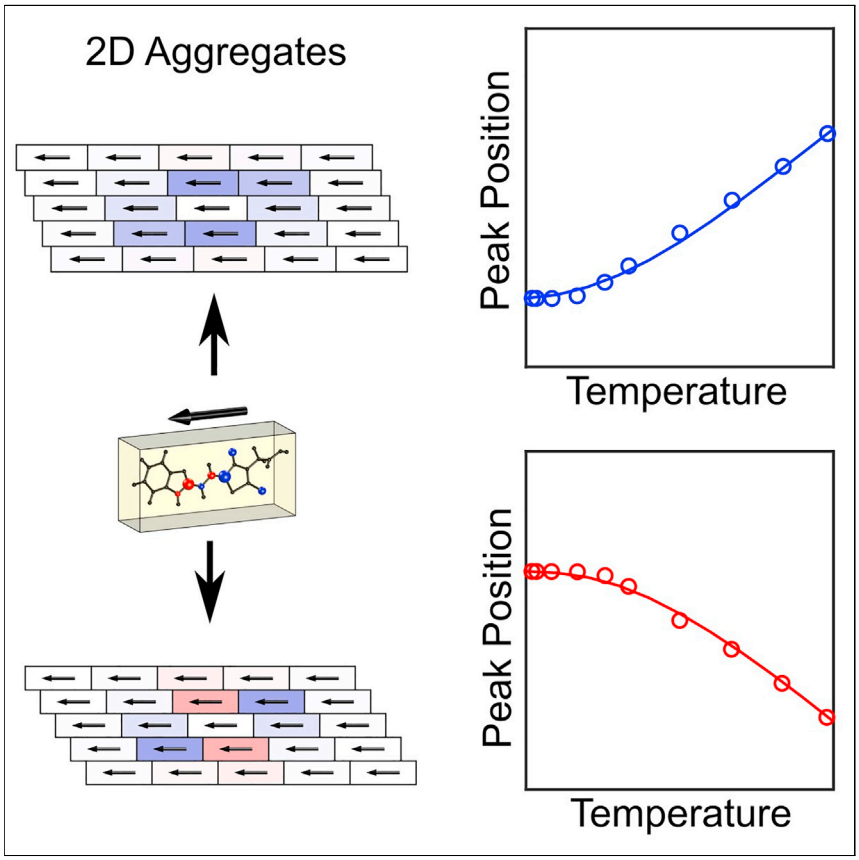

Excitonic organic systems are promising materials for low-cost photovoltaics owing to their tunable absorption profiles. Unfortunately, such tunability often prohibits structural determination tools and hinders the assessment of material properties and the development of design principles. To address this challenge, we provide a conceptual framework relating the temperature-dependent absorption spectra and short-range microscopic structures. This quantitatively accounts for previously unexplained experimental observations and reveals insights in structure-spectroscopic property relationships.

Chern Chuang, Doran I.G. Bennett, Justin R. Caram, Alán Aspuru-Guzik, Moungi G. Bawendi, Jianshu Cao

jianshu@mit.edu

HIGHLIGHTS

We generalize Kasha's theory for excitonic materials with spectral line shapes

Short-range structures are responsible for a temperature-dependent peak shift

A simplified continuum model is provided to visualize the short-range structures

Chuang et al., Chem *5*, 3135–3150
December 12, 2019 © 2019 Elsevier Inc.
https://doi.org/10.1016/j.chempr.2019.08.013

Chem

CellPress

Article

Generalized Kasha's Model: *T*-Dependent Spectroscopy Reveals Short-Range Structures of 2D Excitonic Systems

Chern Chuang,[1] Doran I.G. Bennett,[2,3] Justin R. Caram,[4] Alán Aspuru-Guzik,[2,3,5,6] Moungi G. Bawendi,[1] and Jianshu Cao[1,7,*]

SUMMARY

Excitonic organic materials owe their tunable optoelectronic properties to intricate microscopic configurations, challenging for conventional characterization methods to resolve. We generalize Kasha's model by incorporating the temperature (*T*)-dependent absorption peak shift, in addition to the monomer-aggregate absorption peak shift that defines J- and H-aggregates, to characterize the microscopic structures. We show that the short-range interactions dominate in determining the direction of the *T*-dependent peak shift, which accounts for previously observed *T*-dependent blueshifting J-aggregates (BJ-aggregates) that were not explained and predicts the existence of redshifting H-aggregates (RH-aggregates). This defines four types of excitonic aggregates: RJ-, BH-, BJ-, and RH-aggregates, where the latter two unconventional aggregates are possible because of the two dimensionality of excitonic systems and cannot be understood with the original Kasha's theory. Our conceptual framework is useful for elucidating structure-function relationships in molecular excitonic systems and is fully compatible with existing tools. Possible extensions to other spectroscopic observables and related systems are discussed.

INTRODUCTION

Organic optoelectronic materials have been in the spotlight of energy research for decades.[1–6] These include the study of natural photosynthetic systems composed of proteins and relevant pigments[7,8] as well as artificial devices involving hierarchically self-assembled molecular aggregates.[9] While the photophysical properties of these materials are delicately dependent on the microscopic packing conditions, structure-determination methods such as X-ray diffraction and cryogenic electron microscopy are often inaccessible despite long-range order suggested by optical measurements. As such, indirect methods combining spectroscopy and numerical simulations are generally required to retrieve microscopic structural information and ultimately understand structure-function relationships.[4,10–13]

On the other hand, there are two major challenges that hinder rapid development in such collaborative effort: first, in order to know what structural model to build, we must develop a clear physical intuition connecting microscopic configurations with the photophysics of excitons. Second, in order to rapidly characterize the structural parameters of a given sample, we need to establish spectroscopic signatures that provide unambiguous constraints on structural models. While these challenges have been the subject of numerous recent papers,[4,6,14–23] Kasha's early work on molecular spectroscopy remains the standard for much of the field.[24,25] Here, we

The Bigger Picture

Excitonic organic systems are promising materials for low-cost photovoltaics, owing to their tunable absorption profiles arising from intricate interactions among constituent molecules. Unfortunately, such tunability often prohibits structural determination tools, such as X-ray diffraction or cryo-EM, and hinders the assessment of material properties and the development of design principles.

To address this challenge, we provide a conceptual framework unraveling the link between temperature-dependent absorption peak shift and microscopic structures, generalizing the seminal work of Kasha that defines J/H-aggregates with the packing conditions. We recognize the dominant role of short-range structures in determining the temperature-dependent shift. This quantitatively accounts for previously unexplained experimental observations and reveals insights into structure-spectroscopic property relationships.

extend Kasha's theory to generic low-dimensional excitonic systems and demonstrate that temperature (*T*)-dependent absorption spectroscopy is a powerful discriminator for different microscopic structures and packing conditions.

As mentioned, Kasha's theory was originally developed to explain the significantly redshifted absorption peaks in molecular aggregates, observed for cyanine dyes aggregated in solution compared to monomers by Jelly[26] and Scheibe.[27] By modeling them as dimers or linear chains of molecules interacting through dipolar excitonic couplings, Kasha's theory associates the angle between the transition dipoles and the chain axis directly with the monomer-aggregate absorption peak shift: (1) a redshifted peak corresponds to a head-to-tail configuration, which gives rise to negative excitonic couplings among the dyes, a J-aggregate; and (2) a blueshifted peak corresponds to a side-by-side configuration that leads to positive excitonic couplings, an H-aggregate. This classification of J- and H- aggregates, while providing an ideal example of the physical insights needed to associate microscopic structures with optical measurement, is less useful at inferring the packing conditions for more complicated superstructures that are ubiquitously observed.[6,21,22,28–32] For example, it is found that in the 5,5′,6,6′-tetrachlorobenzimidacarbocyanine dyes of various hydrophilic and hydrophobic side chain lengths, the superstructure varies from linear (1D) to planar (2D), tubular (quasi-1D), or even bundles of tubes (ribbons).[9] For nonlinear superstructures, the incommensurability between the anisotropy of transition dipoles and their local 2D geometry forbids a direct assignment of specific geometric parameters from the monomer-aggregate peak shift.[33–40]

In this contribution, we propose a generalized framework extending Kasha's theory for 1D systems to 2D systems for extracting key microscopic packing parameters. This is possible using *T*-dependent linear spectroscopy and taking into account the direction of the absorption peak shift with increasing temperature, which is easily available experimentally owing to the establishment of sucrose encapsulation methods.[41,42] Using standard line shape theory, we show that in 2D models the *T*-dependent peak shift reveals additional information about its excitonic density of states (DoS) in the vicinity of the bright state, leading to the existence of blueshifting J-aggregates (BJ-aggregates) and redshifting H-aggregates (RH-aggregates) as previously observed experimentally but not explained.[29,43] This is in contrast to 1D models where the absorption peaks of J-aggregates always redshift upon increasing temperature, while the opposite is true for H-aggregates. The direction of the *T*-dependent peak shift, a result of exciton-phonon interactions, is associated with the sign of the total short-range couplings by separately considering the short- and long-range coupling contributions to the excitonic DoS. Specifically, we show that an aggregate with a redshifting absorption peak upon increasing temperature corresponds to one with a net negative short-range coupling. In addition, we show that the long-range coupling is completely determined by a single parameter, the zenith angle of the transition dipole moment with respect to the plane of aggregation. The combination of these principles provides a wealth of unambiguous information on the packing conditions and paves the way to comprehensively understand the structure-function relationships in these systems.

RESULTS AND DISCUSSION

Generalizing Kasha's Model from 1D to 2D

Linear 1D Systems Follow Conventional Kasha's Theory

The preparatory knowledge of the spectral line shape theory is presented in the Experimental Procedures section. In particular, the *T*-dependent absorption peak shift is given by Equation 5. We are now in a position to investigate how different

[1]Department of Chemistry, Massachusetts Institute of Technology, Cambridge, MA 02139, USA

[2]Department of Chemistry and Chemical Biology, Harvard University, Cambridge, MA 02138, USA

[3]Bio-Inspired Solar Energy Program, Canadian Institute for Advanced Research, Toronto, ON M5G 1Z8, Canada

[4]Department of Chemistry and Biochemistry, University of California, Los Angeles, Los Angeles, CA 90095, USA

[5]Department of Chemistry and Department of Computer Science, University of Toronto, Toronto, ON M5S 3H6, Canada

[6]Canada and Vector Institute, Toronto, ON M5G 1M1, Canada

[7]Lead Contact

*Correspondence: jianshu@mit.edu

https://doi.org/10.1016/j.chempr.2019.08.013

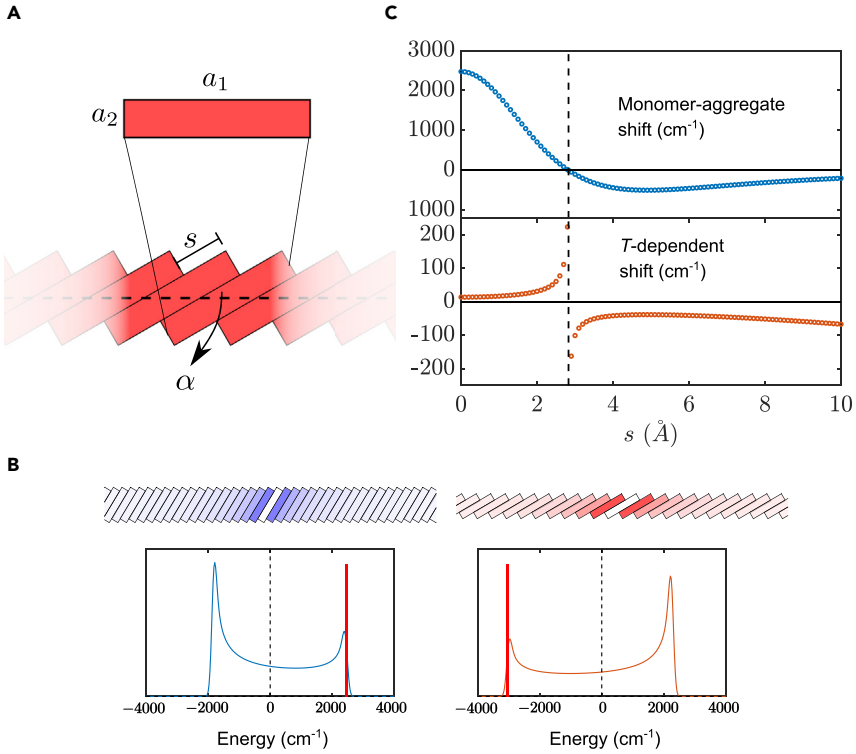

Figure 1. Kasha's model for 1D Excitonic System

(A) Schematic illustration of a 1D excitonic system. s is the offset of adjacent molecular tiles. Here, we set $(a_1, a_2) = (20, 4)$. See text for details.

(B) (Top) Representative J- and H-aggregates in 1D. Red- (blue-) shaded bricks correspond to negative (positive) excitonic dipole-dipole couplings with the molecule at the middle. (Bottom) The corresponding DoS are shown with the vertical lines indicating the locations of the bright states.

(C) (Top) Monomer-aggregate shift calculated with dipole approximation, $\mu_0 = 10$ (Debye). The monomer transition energy is set to zero in all cases. (Bottom) T-dependent peak shift between $T = 0$ and $T = 300$ K, calculated using Equation 5. We use an Ohmic spectral density $J_b(\omega) = \pi\lambda\frac{\omega}{\omega_c}e^{-\omega/\omega_c}$, with reorganization energy $\lambda = 1{,}000$ and cutoff frequency $\omega_c = 1{,}000$ in wavenumber.

microscopic packing conditions lead to different features in the excitonic DoS and therefore the T-dependent peak shift. For linear 1D systems, shown in Figure 1A, a particular configuration can be defined by slip parameter s, an offset in the direction of the molecular long axis between nearest neighbors. The angle between the molecular long axis and the direction of aggregation is $\alpha = 90^\circ - \arctan(s/a_2)$, and $x_0 = a_2\csc\alpha$ is the lattice spacing. Figure 1B shows typical 1D J- and H-aggregates with their corresponding DoS.

In Figure 1C, we present the dependences of both the monomer-aggregate peak shift, $E_b - E_0$ in Equation 2, and the T-dependent peak shift, Equation 5, on the slip parameter s. The former (upper panel) follows Kasha's model, where the monomer-aggregate shift for 1D aggregates can be written as $E_b(\alpha) - E_0 = 2J_{nn}(\alpha)\xi(3)$, where $J_{nn}(\alpha) = C\mu_0^2(1 - 3\cos^2\alpha)/x_0^3$ is the nearest-neighbor coupling strength and $\xi(3) \approx 1.202$ is the Riemann zeta function. μ_0 is the magnitude of the transition dipole in Debye and C is the unit conversion factor. Given the simple dipole form of the excitonic interactions, the excitonic shift is positive (H-aggregates) for smaller s and negative (J-aggregates) for larger ones. The transition occurs at $\alpha = \theta_m = \arccos(1/\sqrt{3}) \approx 54.7^\circ$, the magic angle defined in the context of spectroscopies.

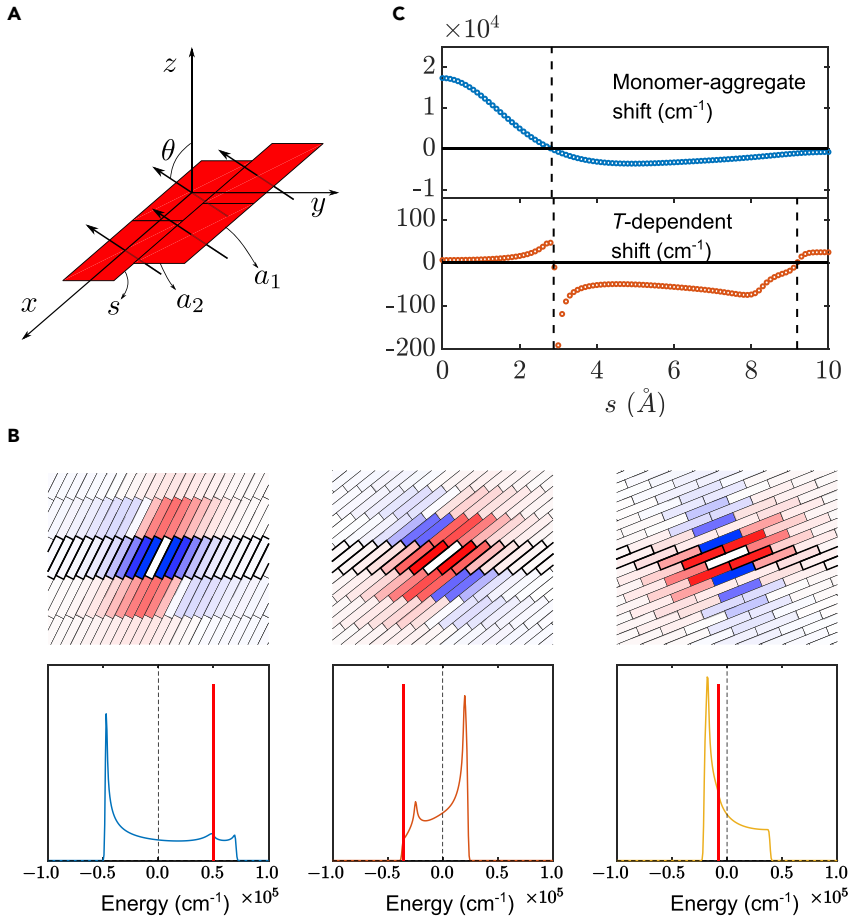

Figure 2. Kasha's model Is Insufficient for 2D Excitonic Systems

(A) Illustration of the 2D brick-layer geometry and the coordinate system.

(B) (Top) Representative 2D aggregates with different slip parameters: s = 2,5,10 from left to right. Red- (blue-) shaded bricks correspond to negative (positive) excitonic dipole-dipole couplings with the molecule at the origin. The 1D aggregates with the same slip parameters are outlined with thick frames. (Bottom) The DoS of the three aggregates drawn on the top. The locations of the bright states $\vec{k} = 0$ are marked by the vertical red lines.

(C) The two-panel configurational space diagram for the 2D aggregates in question. All the conventions follow those in Figure 1C. In all of the aggregates, we adopt the same molecular dimension $(a_1, a_2) = (20, 4)$ and set the zenith angle to be $\theta = 70^\circ$.

We find that 1D J-aggregates that are redshifted compared to the monomers undergo an additional redshift upon increasing temperature ($S(E_b) < 0$), while the opposite is true for 1D H-aggregates ($S(E_b) > 0$). This is also reflected in Equation 6 that all terms in the summation are of the same sign: they are all negative for J-aggregates and all positive for H-aggregates. In other words, the T-dependent peak shift fully correlates with the monomer-aggregate excitonic shift in 1D aggregates and does not provide additional qualitative information with regard to the microscopic packing conditions. Thus, Kasha's original framework suffices to describe both spectroscopic signatures. We shall see how this simple picture is changed in generic 2D systems.

Planar 2D Geometry Supports Novel T-Dependent Properties

By directly extending the corresponding 1D systems to the 2D plane with various slip parameters under the close-packing condition, one can define 2D aggregates as shown in Figure 2A. A defining feature of excitonic 2D systems is the coexistence

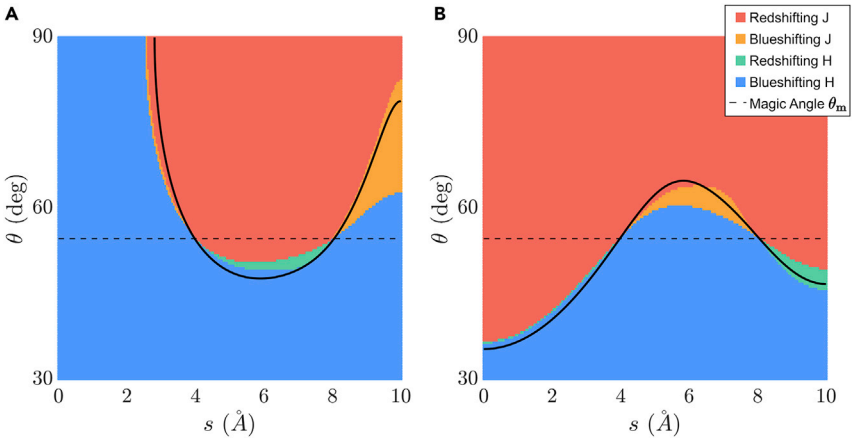

Figure 3. 2D Configurational Space Diagrams of the Four Possible Combinations of Monomer-Aggregate and *T*-Dependent Peak Shifts

The molecular dimension is the same as in previous figures. The horizontal axis is the slip parameter *s*, and the vertical axis is the zenith angle θ.

(A) Transition dipole lying along the long axis (a_1) of the molecular frame.

(B) Transition dipole lying along the short axis (a_2). The solid lines indicate the geometries where the short-range couplings sum to zero. We omit the region $0 < \theta < 30^\circ$ since it is entirely occupied by BH-aggregates. The black line is the solution to $E_b^{(s)}(s,\theta) = 0$, defined in Equation 11.

of positive and negative excitonic couplings.[6,22,30,49] This is with the exception of the case where all transition dipoles point out of the plane of aggregation such that all couplings are positive,[50,51] i.e., a "perfect" H-aggregate. The DoS and the bright state locations corresponding to the lattices shown are presented in the bottom row of Figure 2B. In the left column, we have an H-aggregate (s = 2) while the other two columns to the right (s = 5,10) are J-aggregates.

The *T*-dependent peak shift and the excitonic peak shift no longer follow the same trend, in stark contrast to the 1D systems, as shown in Figure 2C. Notice that the small *s* regions of Figures 1C and 2C are rather similar due to the large aspect ratio a_1/a_2 and the close-packing condition assumed, where the couplings in the horizontal direction (shown in thick frames in Figure 2B) dominate in determining the DoS. However, a novel regime appears at $s > 9.2$, where J-aggregates exist that blueshift upon increasing temperature. J-aggregates with this peculiar property have been reported experimentally but not explained.[29,43] In accordance with our analysis above, the existence of a BJ-aggregate results from larger DoS to the lower energy side of the bright state and a positive slope of the DoS at the bright state. Both of these traits can be seen in the bottom right of Figure 2B.

In addition to the novel BJ-aggregates, it is possible for an RH-aggregate to exist as well. We show this by further exploring the configurational space under the current scheme of close-packing rectangles with two structural parameters: the slip *s* and the zenith angle θ, as shown in Figure 3. In Figure 3A, the in-plane component of the transition dipoles is again set to be parallel to the long axes of the molecules as in most cyanine dyes, while in Figure 3B, the dipoles are parallel to the short axes, exemplified by oligoacenes. Here, all four types of aggregates are recorded: RJ-, BJ-, RH-, and BH-aggregates. In the shorthand notation introduced above, we find $(E_b - E_0) \cdot S(E_b) < 0$ for certain 2D systems that are absent in 1D.

The general trend of monomer-aggregate shift (J or H) along the vertical axis is physically intuitive: the larger the out-of-plane component (small θ), the larger the blue-shift. With increasing θ and closer to the magic angle (Figure 3, dashed horizontal line), however, the dependence on the slip parameter becomes more significant. Also, we find that the two unconventional types, BJ- and RH-aggregates, split perfectly to either side of the magic angle (θ_m). Specifically, BJ-aggregates exist only for $\theta > \theta_m$ and RH-aggregates exist only for $\theta < \theta_m$. While the specific distributions of the J- or H-character and the B- or R-character depend sensitively on both the shape of the molecule and the nature of its transition dipole density, we also find the points of transition between these different characters with the variations of s and θ to constitute smooth and continuous lines in the diagrams.

From Spectroscopy to Microscopic Structures

T-Dependent Peak Shifts Correlate with Short-Range Structures

We emphasize that the lack of perfect correlation between the monomer-aggregate and the T-dependent peak shifts in 2D, observed in Figures 2 and 3, is a direct result of the incommensurability between the anisotropic dipolar coupling and the planar geometry. This ultimately leads to J-aggregates with finite DoS below the bright states and H-aggregates with finite DoS above the bright states. To understand how this is reflected in the microscopic structure of the system, we need to closely examine the dispersion of the exciton energies, especially of its scaling properties near the bright state $k \cdot a \ll 1$, where a is a measure of lattice constant. This is achieved by separating the contribution of short-range interactions from that of the long-range ones, where the latter can be treated using continuum approximation.

$$E_{\vec{k}} = E_0 + \sum_{\vec{n}} J_{\vec{n}} \cos(\vec{k} \cdot \vec{n}) \approx E_0 + E^{(s)}_{\vec{k}} + E^{(l)}_{\vec{k}}, \qquad \text{(Equation 7)}$$

where

$$E^{(s)}_{\vec{k}} = E_{\vec{k}} - E_0 - E^{(l)}_{\vec{k}} \qquad \text{(Equation 8)}$$

and

$$E^{(l)}_{\vec{k}} \approx A\rho_0^2 \int d\vec{r}\, e^{i\vec{k}\cdot\vec{r}}\, \frac{1 - 3\sin^2\theta\cos^2\varphi}{r^3}. \qquad \text{(Equation 9)}$$

In obtaining the long-range continuum result $E^{(l)}_{\vec{k}}$, we treat the couplings as those between a test dipole at the origin and an evenly distributed transition dipole density $\rho_0 = \mu_0/A$, where $A = a_1 a_2$ is the area of the molecule occupied in the 2D plane. Similarly, taking $k \to 0$, we recover the corresponding expression for the bright state energy:

$$\begin{aligned} E_b &= E_0 + \sum_{\vec{n}} J_{\vec{n}} = E_0 + E^{(s)}_b + E^{(l)}_b \\ &= E_0 + E^{(s)}_b + \frac{\pi\rho_0^2 A}{r_c}\left(2 - 3\sin^2\theta\right). \end{aligned} \qquad \text{(Equation 10)}$$

We set a cutoff radius r_c comparable to the dimension of the molecule and an in-plane component parallel to the x axis. In practice, the choice of the cutoff radius r_c depends on the nature of the excitonic coupling, as will be discussed in the next section.

Equation 7 then needs to be connected to the system DoS in order to apply Equation 5. This is achieved with key observations about $E^{(s)}_{\vec{k}}$ and $E^{(l)}_{\vec{k}}$. Because of its

short-range nature, the scaling of $E^{(s)}_{\overrightarrow{k}}$ at $k \cdot a \ll 1$ can be approximated as the cosine form, typical for tight-binding models involving near-neighbor terms. This implies the existence of van Hove singularities, points in the DoS that are not differentiable, near the bright state $\overrightarrow{k} = 0$. These singularities are attenuated by the long-range coupling contribution $E^{(l)}_{\overrightarrow{k}}$ since the band structure of the 2D dipole-dipole interaction in the continuum is known to be linearly dispersed near $\overrightarrow{k} = 0$,[50,51] leading to a smooth and slowly varying contribution to the DoS.

In 2D systems redshifting peaks with increasing temperature occur for packing structures with net negative short-range couplings and blueshifting peaks occur for those with net positive short-range couplings. This follows from the generic scaling property of $E^{(l)}_{\overrightarrow{k}}$ that is insensitive to detailed packing conditions. From this, we deduce that the relative abundance of DoS on either side of the bright state and, therefore, the direction of the *T*-dependent peak shift, is dominated by the short-range contribution to the band structure $E^{(s)}_{\overrightarrow{k}}$. Moreover, this is so regardless of the overall net coupling that defines J- and H- aggregates, $E_b - E_0$. Thus, utilizing Equation 10, we conclude that a key measure that determines the direction of the *T*-dependent peak shift to be

$$E_b^{(s)}(s,\theta) = E_b(s,\theta) - E_0 - \frac{\pi A \rho_0^2}{r_c}\left(2 - 3\sin^2\theta\right), \qquad \text{(Equation 11)}$$

such that systems with $E_b^{(s)} < 0$ redshift and those with $E_b^{(s)} > 0$ blueshift as the temperature increases.

Shown as the solid lines in Figure 3 are the solutions to the equation $E_b^{(s)}(s,\theta) = 0$. Apart from the deviations at large $|\theta - \theta_m|$, Equation 11 correlates quantitatively with the *T*-dependent peak shift, Equation 5. This not only corroborates the connection between the *T*-dependent peak shift and the short-range structures but also serves as a quick assessment without involving line shape calculations. It is also worth mentioning that the red (blue) regions below (above) the dashed lines in Figure 3 are conventional RJ- (BH-) aggregates with short- and long-range couplings of opposite signs. They are related to a class of excitonic materials noted as HJ- or JH-aggregates, discussed in more detailed in The Nature of Short-Range Structures.[6,30]

Since the long-range contribution $E_b^{(l)}$ does not depend on the lattice parameter *s* owing to its continuum nature, it is obvious that the *s* dependence of *T*-dependent peak shift is inherited from the short-range part. However, this argument does not apply to the dependence on θ. To further appreciate the connection between short-range structures and novel *T*-dependent spectroscopic properties, we have to examine the long-range contribution more closely. As demonstrated in the Supplemental Information, only the two conventional aggregates exist for the 2D continuum model with dipole interactions: RJ-aggregates ($\theta_m \le \theta \le \pi/2$) and BH-aggregates ($0 \le \theta < \theta_m$), a situation identical to Kasha's 1D model discussed in the previous section. Thus, we conclude that the nontrivial dependence of *T*-dependent peak shift on (s, θ) in the 2D configurational diagrams is indeed due to the short-range structures.

Spectroscopic Classification Scheme of Microscopic Configurations

We proceed to synthesize our understanding of the monomer-aggregate peak shift and *T*-dependent peak shift and provide a full account of the configurational space

Table 1. All Possible Combinations of the Signs of the Short-Range ($E_b^{(s)}$) and Total Couplings ($E_b - E_0 = E_b^{(s)} + E_b^{(l)}$) in Determining the Monomer-Aggregate and the *T*-dependent Peak Shifts

Type	Short-Range	Total Coupling
RJ	–	–
BJ	+	–
RH	–	+
BH	+	+

diagrams for 2D systems. Starting from the two conventional types, the RJ- and the BH-aggregates, each of them could be the result of two possible combinations of short ($E_b^{(s)}$) and long-range couplings ($E_b^{(l)}$). Firstly, both contributions are of the same sign, which accounts for the case of the RJ- (BH-) aggregate for $\theta > \theta_m$ ($\theta < \theta_m$). Secondly, RJ- (BH-) aggregates could also exist when the two contributions are of opposite signs. To be specific, this happens when the dominant contribution to the excitonic shift is the short-range part. For example, an RJ-aggregate with $\theta < \theta_m$ could result from a lattice structure and transition charge density distribution, supporting strongly negative short-range coupling while maintaining positive long-range coupling. On the one hand, it is a J-aggregate because of the net negative coupling combining the two contributions. On the other hand, it is redshifting due to the short-range contribution being negative. The same argument applies to BH-aggregates with $\theta > \theta_m$.

As for the two unconventional types, the BJ- and RH-aggregates, the situation is reversed. While it is clear that the short- and long-range parts of excitonic coupling are of different signs, the latter is the dominant contribution. However, as the *T*-dependent peak shift is dictated by the short-range couplings, this leads to the novel *T*-dependent properties and the strict separation between the BJ- and the RH-aggregate regions in configurational space by the line $\theta = \theta_m$. The latter strongly supports our framework based on the separation of excitonic couplings into the two parts. We enumerate all possible situations in Table 1.

We note that the long-range couplings are qualitatively determined by a single parameter: the zenith angle θ of the transition dipole moment assuming constant density. This parameter can be assessed robustly by the chemical constitution of the monomers. For example, for the most studied family of excitonic molecular aggregates, amphiphilic cyanine dyes,[9] the hydrophilic and the hydrophobic functional groups are at the sides of the conjugated backbone. This unambiguously defines the plane of aggregation, accommodating a fully in-plane transition dipole moment, i.e., $\theta = 90^\circ$. Other techniques providing access to the value of θ are exemplified by polarization-resolved spectroscopy of Langmuir-Blodgett films[28,29,36] and near-field scanning optical microscopy of pseudoisocyanine (PIC) aggregates.[52] With this information, one can deduce the dominance of either the positive or the negative short-range couplings and narrow down the possible in-plane packing structures of the chromophores.

It has been shown that an RJ-aggregate could in principle possess finite DoS below its bright state, leading to sizable low-*T* line width from the spontaneous phonon contribution (W_0 in Equation 4).[18] Accounting for this additional observable, one can define two subclasses of RJ-aggregates and further generalize the classification scheme, see Supplemental Information for details. Figures S1 and S2 are presented in the same conventions as in Figures 3 and 2C, respectively, with W_0 as an additional variable. We note that a recent analysis on monolayer Perylenetetracarboxylic

dianhydride (PTCDA) molecules on KCl substrate shows non-monotonic *T*-dependence of the superradiance factor.[13] This observation is a sign of such finite DoS below the bright state and warrants further investigation taking advantage of the current framework.

Finally, we note that the limited configurational space volumes occupied by BJ- and RH-aggregates in Figure 3 are likely due to the simple dipole approximation assumed. In our experience, going beyond the dipole approximation often leads to more significant configurational space volumes for the two unconventional aggregates, as exemplified by the example detailed in the following section.

The Nature of Short-Range Structures

In the above sections, we have associated a spectroscopic observable, the *T*-dependent absorption peak shift, directly to the short-range structures of the excitonic materials in question. In the current contribution, we focus our discussion on excitonic interactions of dipole origin, i.e., Frenkel excitons.[1] Therefore, the said short-range structure is due to the discrete nature of the lattice that is not captured by the long-range, continuum approximation employed in Equation 9. In a sense, this coexistence of the short and the long-range couplings makes dipolar interaction a more challenging case. In contrast, there are other non-dipolar sources of short-range interactions that permit straightforward considerations.

Two such possibilities that have been discussed by Spano et al. are (1) charge-transfer mediated[6,22] and (2) bond mediated.[30] In both of these cases, the non-dipolar contributions are by construction short-range and can be seamlessly integrated into our framework, specifically by adding them to the right-hand side of Equation 11. Given the monomer properties (shape and transition charge distribution), configurational space diagrams similar to Figure 3 can then be readily drawn to help connect the *T*-dependent peak shift with packing conditions. It is expected that these additional non-dipolar contributions allow a more robust and direct way to explore the novel *T*-dependent spectroscopic properties.

Next, to account for the non-dipolar couplings, the Spano group has also introduced a shorthand notation for these systems with two letters such as JJ-, HJ-, JH-, and HH-aggregates, with each of the letters referring to the dipolar and the non-dipolar contributions, respectively. In cases that the two contributions are of opposite signs and similar magnitudes, "null aggregates" with vanishing monomer-aggregate shifts arise.[22] In the current context with pure dipolar interactions, analogous situations also exist and correspond to the lines separating the J- (red and orange) and the H-aggregates (green and blue) in Figure 3, where the sum of the long- and short-range contribution vanishes. Generally speaking, an HJ-aggregate could be an overall J- or H-aggregate, depending on the relative strength of the two contributions. It could also be redshifting or blueshifting, depending on the sign and magnitude of the short-range dipolar term. Thus, there is no one-to-one correspondence between the HJ-notation system and the current framework despite similarities at the first sight. This is with the exception of JJ- (HH-) aggregates that cannot possibly be H- (J-) aggregates.

Finally, we note that the complexity of our analysis scales quadratically with the number of transitions involved per unit cell. However, the generic consideration of separating long- and short-range couplings remains a useful technique to determine packing conditions. In essence, the long-range part of Equation 9 can be generalized to cases with *N* transitions per unit cell, by explicitly constructing an *N*-by-*N*

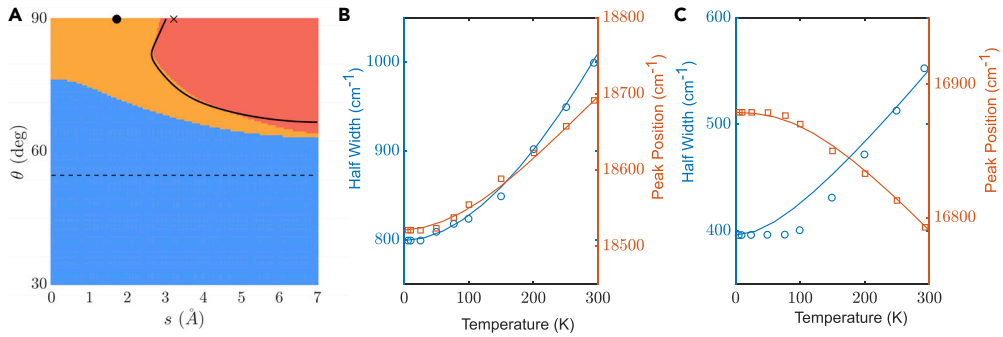

Figure 4. Comparison to Experimental Data of Asymmetric Merocyanine Dye Monolayers

(A) 2D configurational space diagram for the asymmetric merocyanine dyes MC(O) monolayers studied in Yamaguchi et al.[29] The excitonic coupling matrix element $J_{\overrightarrow{n}}$ is calculated using the transition monopole method[60] and the lattice constants $(a_1,a_2) = (14,5)$. The symbols mark the parameters used in Figures 4B and 4C.

(B) The *T*-dependent absorption width (blue circles) and shift (orange squares) of the MC(O) 2D aggregate. The symbols are data taken from experiments and lines are the results of Equations 4 and 5. The lattice parameters are $(s,\theta) = (1.7, 90^\circ)$, marked as the round dot in (A). The phonon bath is described by an Ohmic spectral density with $\omega_c = 1{,}000\ cm^{-1}$ and $\lambda = 3{,}700\ cm^{-1}$. An inhomogeneous broadening of magnitude 110 cm^{-1} is added to the absorption width.

(C) The *T*-dependent spectral trends for the MC(S) 2D aggregate, with lattice parameters $(s,\theta) = (3.2, 90^\circ)$, marked as the cross in (A). An Ohmic bath with $\omega_c = 1{,}000\ cm^{-1}$ and $\lambda = 1{,}400\ cm^{-1}$ and an inhomogeneous gaussian broadening with width 350 cm^{-1} are used. The transition charge distributions for MC(S) and MC(Se) dyes are similar to that of the MC(O)'s (data not shown).

coupling matrix in the *k*-space. It is also worth mentioning that albeit we assume homogeneity in the current framework, we expect the framework to hold for cases with finite static disorder. This is because the short-range structures are more resilient to the influence of disorder, a known observation in the study of Anderson localization.[53] These topics are currently under our investigation.

Comparison to Experiments: Merocyanine Dye Monolayers

With the conceptual framework established, it is helpful to apply it to real systems. In Figure 4, we study the *T*-dependent absorption peak width and shift of asymmetric merocyanine dye monolayers that have been characterized experimentally.[29] Three different dyes with similar structures are considered: MC(X) (X=O, S, or Se). While all three dyes form J-aggregate monolayers, it is most noteworthy that the MC(O) monolayer shows a different *T*-dependent trend compared to the other two. Specifically, the MC(O) monolayer absorption peak blueshifts with increasing temperature, an example of a 2D BJ-aggregate.

In Figure 4A, we show the 2D configurational space diagram of the MC(O) monolayer. While the lattice structure is similar to that adopted in Figure 3A with the transition dipole parallel to the molecular long axis, we find no configuration corresponding to an RH-aggregate. This is likely due to the nature of the transition charge distribution of the merocyanine dye molecules forbidding strongly negative short-range couplings. Consequently, the solid line corresponding to $E_b^{(s)}(s,\theta) = 0$ nearly overlaps with the boundary of RJ-aggregate configurational space. In Figures 4B and 4C, we show the comparisons between the experimental *T*-dependent line shapes of MC(O) and MC(S) monolayers and those from Equations 4 and 5. In both cases, we set $\theta = 90^\circ$, while the corresponding slip parameters are marked. While there are quantitative agreements between experiment and simulation in general, we find noticeable deviation of low temperature absorption width in the MC(S) case. This is attributed to the *ad hoc* treatment of sizable static disorder and will be addressed in our future work.

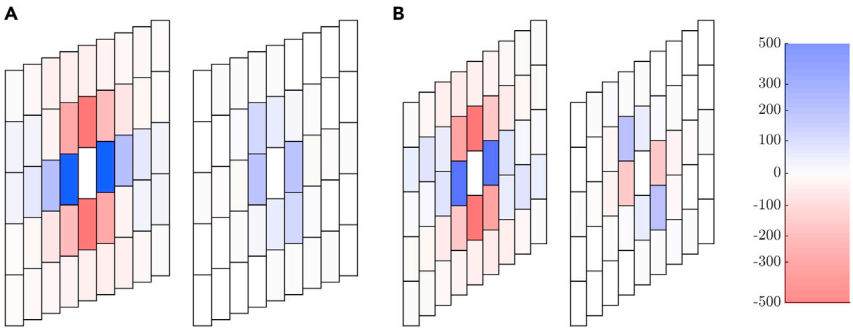

Figure 5. The Comparison between the Full Couplings (Left) and the Short-Range Couplings (Right) Given by the Continuum Brick Model in Equation 13 for the Merocyanine Dyes
(A) MC(O), BJ-aggregate.
(B) MC(S), RJ-aggregate.

While the *T*-dependent peak shift reflects the sum total of the short-range couplings $E_b^{(s)}$, it will be useful to spatially resolve the individual coupling terms on a given lattice. For this purpose, we introduce an approximate but illuminating model, the continuum brick model. Detailed in the Supplemental Information, this model essentially groups the transition dipole coupling within a rectangular brick of the continuum model and concentrates the coupling strength onto the corresponding lattice point. As such, the long-range couplings can be defined as

$$J_{\vec{n}}^{c.b.} = \frac{\mu_0^2}{A} \int_{A_{\vec{n}}} d\vec{r} \cdot \frac{1 - 3\sin^2\theta\cos^2\varphi}{r^3}, \qquad \text{(Equation 12)}$$

where $A_{\vec{n}}$ is the area occupied by the $\vec{n}$th rectangular brick and φ is the azimuth angle of the transition dipole moment. Consequently, the residual, short-range couplings are

$$J_{\vec{n}}^{(s)} \approx J_{\vec{n}} - J_{\vec{n}}^{c.b.}. \qquad \text{(Equation 13)}$$

The results are presented in Figure 5, where we take the MC(O) and the MC(S) monolayers examined above and apply Equations 12 and 13. We observe that $J_{\vec{n}}^{(s)}$ (right panels) are indeed short ranged. Note that not only are the coupling magnitudes altered, but the signs of certain couplings are also flipped compared to the original, full couplings. Since both of them are J-aggregates, the summations over all bricks that define the monomer-aggregate peak shift are negative in both cases. For the MC(O) monolayer, a BJ-aggregate shown in Figure 5A, the short-range couplings defined in Equation 13 are dominantly positive, leading to $E_b^{(s)}>0$. The opposite is true for the MC(S) monolayer, an RJ-aggregate shown in Figure 5B. This corroborates our prediction that the sign of the short-range couplings is the determining factor of the temperature-dependent peak shift.

It is possible to generalize the current framework to related excitonic systems. Firstly, by suitably accounting for the boundary condition, an expression similar to Equation 9 is derived for tubular aggregates that have received much attention recently,[17–19,32,39,40,42] which will be discussed extensively in our forthcoming work. Also, in addition to dye aggregates and crystals, systems with significant excitonic interactions including pigment-based metal-organic frameworks[54] and quantum dot superlattices[55] are possible examples for such extension as well. On the other hand, strong excitonic interactions do not necessarily assure a straightforward

application of the current framework. For example, in conjugated polymers such as polythiophene, a blueshift of absorption peak with increasing temperature has been shown to result from the reduction of effective conjugation length in these systems at elevated temperatures.[56] Also, a recent experimental study of clean suspended $MoSe_2$ monolayers reports a redshift with increasing temperature.[57] While the monomer-aggregate peak shift is not well defined in these covalently bonded extended systems, we point out that the exciton band structures of direct bandgap 2D materials resemble those of RJ-aggregates in the current context, where the exciton dispersion bends upward with increasing momentum near $\vec{k} = 0$.[58,59]

Conclusions

We present a generalized conceptual framework for excitonic molecular systems based on an analysis of spectroscopic observables. In the framework, the original model of Kasha is expanded to include the *T*-dependent spectral shift in addition to the monomer-aggregate peak shift. Using standard spectral line shape theory, we explain the origin of a class of J-aggregates that blueshift with increasing temperature (BJ-aggregates) previously observed experimentally. In addition, another novel class of RH-aggregates, not yet reported to the best of our knowledge, is predicted together with configurations that might produce such cases. The *T*-dependent peak shift is directly related to the relative location of the bright state in the system DoS, which derives from the excitonic band structure. The usefulness of the generalized framework is most apparent when considering the direction of the *T*-dependent peak shift as a key observable, with the magnitude of the shift quantified by Equation 5.

We further establish the connection between the excitonic DoS and the microscopic configurations, given the knowledge of both the monomer-aggregate and the *T*-dependent peak shifts. This is achieved by separating the contributions to the exciton band structure into long- and short-range coupling terms. The long-range contribution provides a smooth background for the DoS and is dictated by a single parameter θ, the zenith angle between the transition dipole moment, and the z axis. On the other hand, the short-range contribution is the dominant factor in determining the direction of the *T*-dependent peak shift. Specifically, a net negative short-range coupling gives rise to a redshifting aggregate, whereas a net positive total short-range coupling leads to a blueshifting aggregate. Detailed analysis together with the knowledge of θ further distinguish the conventional RJ- and BH-aggregates into four classes depending on synergy between the short- and the long-range couplings.

Our generalized framework uses experimentally accessible information including *T*-dependent linear absorption and polarization-resolved spectroscopy and reveals microscopic configurations of 2D systems as in Kasha's original theory for 1D systems. Additional information can also be seamlessly integrated, such as the inclusion of non-dipolar interactions or charge-transfer (CT)-mixed contributions that alter the short-range coupling but decouple from the long-range part. Our work is useful in deciphering aggregate geometries that evade traditional high-resolution structure-determination techniques such as X-ray scattering and may provide a set of design principles for excitonic systems with desired spectroscopic properties.

EXPERIMENTAL PROCEDURES

Computational Method

Our consideration starts from the standard Frenkel exciton model

$$\widehat{H}^{(s)} = \sum_{\vec{n}} E_{\vec{n}} |\vec{n}\rangle\langle\vec{n}| + \sum_{\vec{n}\neq\vec{m}} J_{\vec{n},\vec{m}} |\vec{n}\rangle\langle\vec{m}|, \quad \text{(Equation 1)}$$

where $E_{\vec{n}}$ and $J_{\vec{n},\vec{m}}$ are the site energy and the excitonic coupling, respectively, and $|\vec{n}\rangle$ represents the state where the designated site is in the excited state while all other sites are in the ground state. By assuming the homogeneous limit and periodic boundary condition, i.e., $E_{\vec{n}} = E_0$ and $J_{\vec{n},\vec{m}} = J_{\vec{n}-\vec{m}}$, the location of the bright state is given by

$$E_b = E_0 + \sum_{\vec{n}} J_{\vec{n}}. \quad \text{(Equation 2)}$$

The central quantity concerned in Kasha's theory, the monomer-aggregate absorption peak shift, is $E_b - E_0 = \sum_n J_n$. More generally, the Hamiltonian Equation 1 can be diagonalized with Bloch waves $\left|\vec{k}\right\rangle = \sum_{\vec{n}} e^{i\vec{k}\cdot\vec{n}} \left|\vec{n}\right\rangle$, leading to the exciton dispersion relation $E = E_{\vec{k}}$. With this, one can define the DoS for the excitonic system $D^{(s)}(E) = \sum_{\vec{k}} \delta(E - E_{\vec{k}})$.

While E_b indicates the location of the bright state when the molecule is in isolation, the phonon environment of the excitons broadens and shifts absorption line shapes. This environment is represented by a distribution of harmonic oscillators coupled to the excitons. We adopt the standard Redfield description of the exciton-phonon interaction, detailed in the Supplemental Information. We further assume the secular and Markovian approximations. In the former, we assume that the phonon-induced population relaxation is the dominant dephasing process, while in the latter the phonon environment is taken to be relaxing faster than the excitonic system. This method has been shown to properly account for linear absorption line shapes of excitonic molecular aggregates in most circumstances.[44] The line shape of the bright state is given by a Lorentzian function[44–47]

$$A(E) = \frac{1}{[E - E_b - S(E_b)]^2 + \left[\frac{1}{2}W(E_b)\right]^2}, \quad \text{(Equation 3)}$$

where

$$W(E) = \int dE' \cdot D^{(s)}(E') J^{(b)}(|E - E'|)^{-} n_{BE}(|E - E'|) + W_0(E) \quad \text{(Equation 4)}$$

and

$$S(E) = \frac{2}{\pi} \int dE' D^{(s)}(E')(E - E') \cdot \mathcal{P} \int_0^{\infty} dE'' \frac{J^{(b)}(E'')^{-} n_{BE}(E'')}{E''^2 - (E - E')^2} + S_0(E), \quad \text{(Equation 5)}$$

where $J^{(b)}(E)$ is the bath spectral density and ${}^{-}n_{BE}(E)$ is the Bose-Einstein distribution. $\mathcal{P}$ stands for the Cauchy principal value of the integral. W_0 and S_0 are the T-independent components detailed in the Supplemental Information. While Equation 4 has been obtained by Heijs et al.[48] and utilized to explain the power-law scaling of T-dependent absorption line width, Equation 5 is the main focus of the current contribution.

A few comments are due in connecting the above formulation to experimental observables. Firstly, Equation 3 describes a peak located at $E_b + S(E_b)$ with a full width at half maximum $W(E_b)$. Secondly and most importantly, while the width W monotonically increases with increasing temperature, the sign of the T-dependent peak shift is dictated by the relative abundance of system DoS to the higher and the lower energy side of the bright state, weighted by the bath spectral density and phonon thermal occupation numbers. This is owing to the asymmetry of the dependence on energy gap $E - E'$ in Equation 5. More specifically, this expression predicts that DoS higher in energy than the bright state effectively pushes it away, inducing a redshift with increasing temperature, whereas DoS lower in energy than the bright state induces a blueshift with increasing temperature. We note that this is similar to the effects of static disorder, as is discussed in our earlier paper, where the second-order correction to the system eigenstate energy is[42]

$$\Delta E_k = \sum_{l \neq k} \frac{\left|\langle l|V(T)|k\rangle\right|^2}{E_k - E_l}, \qquad \text{(Equation 6)}$$

where $V(T)$ is the system part of the system-bath interaction averaged over the thermal distribution of the bath, a monotonically increasing function of T. As mentioned, this expression gives a naive but intuitive connection between the phonon-induced peak shift and the system DoS. This effect is additive, as the net T-dependent peak shift is determined by whichever side has a larger weighted system DoS in Equation 5. In cases where the DoS is differentiable, this leads to the notion that the absorption peak redshifts with increasing temperature if the slope of the DoS is positive $\left.\frac{dD^{(s)}(E)}{dE}\right|_{E=E_b} > 0$ and vice versa. This proves very useful in the generalized framework proposed below and can be utilized to explain experimental results previously observed that are not accounted for by Kasha's original model, detailed in the Results and Discussion section.

We further note that our method does not take full account of the line shape of the absorption peaks such as vibronic progressions, which can be useful to retrieving microscopic information.[15] While such consideration warrants a separate report, in a zeroth order picture, we predict that the mean position of a progression shifts according to the same fashion described above. In general, the peak shift discussed in the current work can be seen as a renormalization of excitonic couplings by exciton-phonon interactions. It is expected that nontrivial vibronic structures might quantitatively change this picture. In addition, we note that nonlinear spectroscopies that take into account diverse relaxation pathways provide further information still.[14,19]

SUPPLEMENTAL INFORMATION

Supplemental Information can be found online at https://doi.org/10.1016/j.chempr.2019.08.013.

ACKNOWLEDGMENTS

J.C. acknowledges the support from the National Science Foundation (grant nos. CHE 1836913 and CHE 1800301). J.R.C. was funded by the US Department of Energy, Office of Basic Energy Sciences, and Division of Materials Sciences and Engineering (award no. DE-FG02-07ER46454).

AUTHOR CONTRIBUTIONS

Conceptualization, C.C., D.I.G.B., J.R.C., and J.C.; Methodology, C.C. and J.C.; Formal Analysis, C.C.; Investigation, C.C., D.I.G.B., J.R.C., and J.C.; Writing – Original Draft, C.C.; Writing – Review & Editing, C.C., D.I.G.B., J.R.C., and J.C.; Supervision, A.A.-G, M.G.B., and J.C.

DECLARATION OF INTERESTS

The authors declare no competing interests.

Received: May 13, 2019
Revised: July 13, 2019
Accepted: August 20, 2019
Published: September 16, 2019

REFERENCES AND NOTES

1. Davydov, A.S. (1971). Theory of Molecular Excitons (Springer).
2. Kenkre, V.M., and Reineker, P. (1982). Exciton Dynamics in Molecular Crystals and Aggregates, *Volume 94* (Springer).
3. Möbius, D. (1995). Scheibe aggregates. Adv. Mater. *7*, 437–444.
4. Würthner, F., Kaiser, T.E., and Saha-Möller, C.R. (2011). J-aggregates: from serendipitous discovery to supramolecular engineering of functional dye materials. Angew. Chem. Int. Ed. Engl. *50*, 3376–3410.
5. Bardeen, C.J. (2014). The structure and dynamics of molecular excitons. Annu. Rev. Phys. Chem. *65*, 127–148.
6. Hestand, N.J., and Spano, F.C. (2017). Molecular aggregate photophysics beyond the kasha model: novel design principles for organic materials. Acc. Chem. Res. *50*, 341–350.
7. Cogdell, R.J., Gardiner, A.T., Gabrielsen, M., Southall, J., Roszak, A.W., Isaacs, N.W., Fujii, R., and Hashimoto, H. (2008). The structure of purple bacterial antenna complexes. In Photosynthetic Protein Complexes: A Structural Approach, P. Fromme, ed. (Wiley-VCH Verlag GmbH & Co. KGaA), pp. 325–340.
8. Blankenship, R.E., Tiede, D.M., Barber, J., Brudvig, G.W., Fleming, G., Ghirardi, M., Gunner, M.R., Junge, W., Kramer, D.M., Melis, A., et al. (2011). Comparing photosynthetic and photovoltaic efficiencies and recognizing the potential for improvement. Science *332*, 805–809.
9. Kirstein, S., and Daehne, S. (2006). J-aggregates of amphiphilic cyanine dyes: self-organization of artificial light harvesting complexes. Int. J. Photoenergy *2006*, 1–21.
10. Pawlik, A., Kirstein, S., De Rossi, U., and Daehne, S. (1997). Structural conditions for spontaneous generation of optical activity in J-aggregates. J. Phys. Chem. B *101*, 5646–5651.
11. Müller, M., Paulheim, A., Eisfeld, A., and Sokolowski, M. (2013). Finite size line broadening and superradiance of optical transitions in two dimensional long-range ordered molecular aggregates. J. Chem. Phys. *139*, 044302.
12. Liess, A., Lv, A., Arjona-Esteban, A., Bialas, D., Krause, A.M., Stepanenko, V., Stolte, M., and Würthner, F. (2017). Exciton coupling of merocyanine dyes from H- to J-type in the solid state by crystal engineering. Nano Lett. *17*, 1719–1726.
13. Eisfeld, A., Marquardt, C., Paulheim, A., and Sokolowski, M. (2017). Superradiance from two dimensional brick-wall aggregates of dye molecules: the role of size and shape for the temperature dependence. Phys. Rev. Lett. *119*, 097402.
14. Sperling, J., Nemeth, A., Hauer, J., Abramavicius, D., Mukamel, S., Kauffmann, H.F., and Milota, F. (2010). Excitons and disorder in molecular nanotubes: a 2d electronic spectroscopy study and first comparison to a microscopic model. J. Phys. Chem. A *114*, 8179–8189.
15. Spano, F.C. (2010). The spectral signatures of Frenkel polarons in H- and J-aggregates. Acc. Chem. Res. *43*, 429–439.
16. Tian, Y., Camacho, R., Thomsson, D., Reus, M., Holzwarth, A.R., and Scheblykin, I.G. (2011). Organization of bacteriochlorophylls in individual chlorosomes from Chlorobaculum tepidum studied by 2-dimensional polarization fluorescence microscopy. J. Am. Chem. Soc. *133*, 17192–17199.
17. Eisele, D.M., Cone, C.W., Bloemsma, E.A., Vlaming, S.M., van der Kwaak, C.G.F., Silbey, R.J., Bawendi, M.G., Knoester, J., Rabe, J.P., and Vanden Bout, D.A. (2012). Utilizing redox-chemistry to elucidate the nature of exciton transitions in supramolecular dye nanotubes. Nat. Chem. *4*, 655–662.
18. Wan, Y., Stradomska, A., Fong, S., Guo, Z., Schaller, R.D., Wiederrecht, G.P., Knoester, J., and Huang, L. (2014). Exciton level structure and dynamics in tubular porphyrin aggregates. J. Phys. Chem. C *118*, 24854–24865.
19. Abramavicius, D., Nemeth, A., Milota, F., Sperling, J., Mukamel, S., and Kauffmann, H.F. (2012). Weak exciton scattering in molecular nanotubes revealed by double-quantum two-dimensional electronic spectroscopy. Phys. Rev. Lett. *108*, 067401.
20. Eisenberg, I., Yochelis, S., Ben-Harosh, R., David, L., Faust, A., Even-Dar, N., Taha, H., Haegel, N.M., Adir, N., Keren, N., et al. (2014). Room temperature biological quantum random walk in phycocyanin nanowires. Phys. Chem. Chem. Phys. *16*, 11245–11250.
21. Dijkstra, A.G., Duan, H.G., Knoester, J., Nelson, K.A., and Cao, J. (2016). How two-dimensional brick layer J-aggregates differ from linear ones: excitonic properties and line broadening mechanisms. J. Chem. Phys. *144*, 134310.
22. Hestand, N.J., and Spano, F.C. (2018). Expanded theory of H- and J-molecular aggregates: the effects of vibronic coupling and intermolecular charge transfer. Chem. Rev. *118*, 7069–7163.
23. Deshmukh, A.P., Koppel, D., Chuang, C., Cadena, D.M., Cao, J., and Caram, J.R. (2019). Design principles for two-dimensional molecular aggregates using Kasha's model: tunable photophysics in near and short-wave infrared. J. Phys. Chem. C *123*, 18702–18710.
24. Kasha, M. (1963). Energy transfer mechanisms and the molecular exciton model for molecular aggregates. Radiat. Res. *20*, 55–70.
25. Kasha, M., Rawls, H.R., and El-Bayoumi, M.A. (1965). The exciton model in molecular spectroscopy. Pure Appl. Chem. *11*, 371–392.
26. Jelley, E.E. (1936). Spectral absorption and fluorescence of dyes in the molecular state. Nature *138*, 1009–1010.
27. Scheibe, G. (1937). Über die Veränderlichkeit der Absorptionsspektren in Lösungen und die Nebenvalenzen als ihre Ursache. Angew. Chem. *50*, 212–219.
28. Nabetani, A., Tomioka, A., Tamaru, H., and Miyano, K. (1995). Optical properties of two-dimensional dye aggregate. J. Chem. Phys. *102*, 5109–5117.
29. Yamaguchi, A., Kometani, N., and Yonezawa, Y. (2006). Spectroscopic properties of the mixed J-aggregate of unsymmetric merocyanine dyes in wide temperature range. Thin Solid Films *513*, 125–135.

30. Yamagata, H., and Spano, F.C. (2012). Interplay between intrachain and interchain interactions in semiconducting polymer assemblies: the HJ-aggregate model. J. Chem. Phys. *136*, 184901.

31. Arias, D.H., Stone, K.W., Vlaming, S.M., Walker, B.J., Bawendi, M.G., Silbey, R.J., Bulović, V., and Nelson, K.A. (2013). Thermally-limited exciton delocalization in superradiant molecular aggregates. J. Phys. Chem. B *117*, 4553–4559.

32. Barclay, T.G., Constantopoulos, K., and Matisons, J. (2014). Nanotubes self-assembled from amphiphilic molecules via helical intermediates. Chem. Rev. *114*, 10217–10291.

33. Czikkely, V., Försterling, H.D., and Kuhn, H. (1970). Light absorption and structure of aggregates of dye molecules. Chem. Phys. Lett. *6*, 11–14.

34. Blaudez, D., Buffeteau, T., Desbat, B., Orrit, M., and Turlet, J.M. (1992). Characterization of Langmuir-Blodgett monolayers using polarization modulated FTIR spectroscopy. Thin Solid Films *210–211*, 648–651.

35. Kuhn, H., and Möbius, D. (1993). Monolayer assemblies. In Physical Methods of Chemistry 9, Part B, Investigations of Surfaces and Interfaces, B.W. Rossiter and R.C. Baetzold, eds. (Wiley).

36. Hsu, Y., Penner, T.L., and Whitten, D.G. (1994). Polarized spectroscopic studies of ferrocenyl Langmuir-Blodgett assemblies. Langmuir *10*, 2757–2765.

37. Gil, A., Möbius, D., Sández, I., and Suárez, A. (2003). Different J-aggregates of an amphiphilic cyanine dye in monolayers at the air-water interface. Langmuir *19*, 6430–6435.

38. Aviv, H., and Tischler, Y.R. (2015). Synthesis and characterization of a J-aggregating TDBC derivative in solution and in Langmuir-Blodgett films. J. Lumin. *158*, 376–383.

39. Li, X., Buda, F., de Groot, H.J.M., and Sevink, G.J.A. (2018). Contrasting modes of self-assembly and hydrogen-bonding heterogeneity in chlorosomes of Chlorobaculum tepidum. J. Phys. Chem. C Nanomater Interfaces *122*, 14877–14888.

40. Löhner, A., Kunsel, T., Röhr, M.I.S., Jansen, T.L.C., Sengupta, S., Würthner, F., Knoester, J., and Köhler, J. (2019). Spectral and structural variations of biomimetic light-harvesting nanotubes. J. Phys. Chem. Lett. *10*, 2715–2724.

41. Caram, J.R., Doria, S., Eisele, D.M., Freyria, F.S., Sinclair, T.S., Rebentrost, P., Lloyd, S., and Bawendi, M.G. (2016). Room-temperature micron-scale exciton migration in a stabilized emissive molecular aggregate. Nano Lett. *16*, 6808–6815.

42. Doria, S., Sinclair, T.S., Klein, N.D., Bennett, D.I.G., Chuang, C., Freyria, F.S., Steiner, C.P., Foggi, P., Nelson, K.A., Cao, J., et al. (2018). Photochemical control of exciton superradiance in light-harvesting nanotubes. ACS Nano *12*, 4556–4564.

43. Kaiser, T.E., Scheblykin, I.G., Thomsson, D., and Würthner, F. (2009). Temperature-dependent exciton dynamics in J-aggregates - when disorder plays a role. J. Phys. Chem. B *113*, 15836–15842.

44. Ma, J., and Cao, J. (2015). Förster resonance energy transfer, absorption and emission spectra in multichromophoric systems. I. Full cumulant expansions and system-bath entanglement. J. Chem. Phys. *142*, 094106.

45. Mukamel, S. (1995). The Principles of Nonlinear Optical Spectroscopy (Oxford).

46. Cleary, L., and Cao, J. (2013). Optimal thermal bath for robust excitation energy transfer in disordered light-harvesting complex 2 of purple bacteria. New J. Phys. *15*.

47. Moix, J.M., Ma, J., and Cao, J. (2015). Förster resonance energy transfer, absorption and emission spectra in multichromophoric systems. III. Exact stochastic path integral evaluation. J. Chem. Phys. *142*, 094108.

48. Heijs, D.J., Malyshev, V.A., and Knoester, J. (2005). Thermal broadening of the J-band in disordered linear molecular aggregates: a theoretical study. J. Chem. Phys. *123*, 144507.

49. Cleary, L., Chen, H., Chuang, C., Silbey, R.J., and Cao, J. (2013). Optimal fold symmetry of LH2 rings on a photosynthetic membrane. Proc. Natl. Acad. Sci. USA *110*, 8537–8542.

50. Christiansen, P.L., Gaididei, Y.B., Johansson, M., Rasmussen, K.Ø., Mezentsev, V.K., and Rasmussen, J.J. (1998). Solitary excitations in discrete two-dimensional nonlinear Schrödinger models with dispersive dipole-dipole interactions. Phys. Rev. B *57*, 11303–11318.

51. Domínguez-Adame, F., Malyshev, V.A., and Rodríguez, A. (2000). Absorption spectra of dipolar Frenkel excitons in two-dimensional lattices with configurational disorder: long-range interaction and motional narrowing effects. J. Chem. Phys. *112*, 3023–3030.

52. Reid, P.J., Higgins, D.A., and Barbara, P.F. (1996). Environment-dependent photophysics of polymer-bound J-aggregates determined by time-resolved fluorescence spectroscopy and time-resolved near-field scanning optical microscopy. J. Phys. Chem. *100*, 3892–3899.

53. Malyshev, V., and Moreno, P. (1995). Hidden structure of the low-energy spectrum of a one-dimensional localized Frenkel exciton. Phys. Rev. B Condens Matter *51*, 14587–14593.

54. Son, H.J., Jin, S., Patwardhan, S., Wezenberg, S.J., Jeong, N.C., So, M., Wilmer, C.E., Sarjeant, A.A., Schatz, G.C., Snurr, R.Q., et al. (2013). Light-harvesting and ultrafast energy migration in porphyrin-based metal-organic frameworks. J. Am. Chem. Soc. *135*, 862–869.

55. Rainò, G., Becker, M.A., Bodnarchuk, M.I., Mahrt, R.F., Kovalenko, M.V., and Stöferle, T. (2018). Superfluorescence from lead halide perovskite quantum dot superlattices. Nature *563*, 671–675.

56. Kanemoto, K., Akai, I., Sugisaki, M., Hashimoto, H., Karasawa, T., Negishi, N., and Aso, Y. (2009). Temperature effects on quasi-isolated conjugated polymers as revealed by temperature-dependent optical spectra of 16-mer oligothiophene diluted in a sold matrix. J. Chem. Phys. *130*, 234909.

57. Scuri, G., Zhou, Y., High, A.A., Wild, D.S., Shu, C., De Greve, K., Jauregui, L.A., Taniguchi, T., Watanabe, K., Kim, P., et al. (2018). Large excitonic reflectivity of monolayer $MoSe^2$ encapsulated in hexagonal boron nitride. Phys. Rev. Lett. *120*, 037402.

58. Qiu, D.Y., Cao, T., and Louie, S.G. (2015). Nonanalyticity, valley quantum phases, and lightlike exciton dispersion in monolayer transition metal dichalcogenides: theory and first-principles calculations. Phys. Rev. Lett. *115*, 176801.

59. Wang, G., Chernikov, A., Glazov, M.M., Heinz, T.F., Marie, X., Amand, T., and Urbaszek, B. (2018). Colloquium: excitons in atomically thin transition metal dichalcogenides. Rev. Mod. Phys. *90*.

60. Chen, C.T., Chuang, C., Cao, J., Ball, V., Ruch, D., and Buehler, M.J. (2014). Excitonic effects from geometric order and disorder explain broadband optical absorption in eumelanin. Nat. Commun. *5*, 3859.